NUMERICAL AND EXPERIMENTAL STUDY OF THE MODE I INTERLAMINAR FAILURE OF CHOPPED CARBON FIBER TAPE REINFORCED THERMOPLASTICS

Qitao Guo, Bohan Xiao, Ye Zhang, Bijan Spitzlei, Isamu Ohsawa and Jun Takahashi
Department of Systems Innovation, The University of Tokyo, Japan
Email: guo-qitao@cfrtp.t.u-tokyo.ac.jp

Keywords: Discontinuous CFRTP, Double Cantilever Beam, Interlaminar failure

ABSTRACT

Carbon fiber reinforced plastics (CFRP) are increasingly used in primary structural components of automobile and aircrafts on count of their high specific modulus and strength. For this reason, they have attracted much attention of researchers, industrial manufacturers and even the general public. Randomly oriented carbon fiber reinforced thermoplastics (Randomly oriented CFRTP), in particular chopped carbon fiber tape reinforced thermoplastics (CTT), have been current research focus due to its advantageous properties such as high-productivity and design flexibility that are not attainable from conventional material. Besides, the mass application of randomly oriented CFRTP in automotive industry has been regarded as potential solution to reduce resource shortage and environmental pollution.

Interlaminar failure, however, causes significant reduction on the load carrying capacity of fiber-reinforced composites, which is a major concern to aerospace and automotive industries. The interlaminar fracture energy release rate of fiber-reinforced composites can be measured for any of the three possible crack propagation modes: opening mode (Mode I), shear mode (Mode II) and tearing mode (Mode III), and Mode I is the most critical crack propagation mode because it has the lowest associated fracture energy release rate. Many researches have focused on interlaminar failure of woven composites and unidirectional carbon fiber epoxy composites by using numerical and experimental analysis, but few studies about interlaminar failure of randomly oriented CFRTP can be found.

In the present study, the Mode I interlaminar failure of CTT specimen was investigated during double cantilever beam (DCB) tests in which the crosshead was moved at a constant speed of 1mm/min. In order to measure the compliance of the specimen, it was unloaded after each significant crack propagation during testing. The results show an unstable crack growth resulting in a saw-tooth like force-displacement curve after initial linear stage. The mode I energy release rate was determined by three different analytical calculation methods: modified compliance calibration (MCC), modified beam theory (MBT) and beam theory in reference to JIS K 7086 standard. Furthermore, DCB specimen was modeled to capture the fracture behavior. The numerical results are in good agreement with the experimental results suggesting the finite element model can be used to simulate the delamination process.

1. INTRODUCTION

Carbon fiber reinforced plastics (CFRP) are increasingly used in primary structural components of automobile and aircrafts on count of their high specific modulus and strength. However, the limitations of high manufacturing costs and complex shape formability difficulty of the conventionally used continuous fiber composites have limited their mass-produced applications. Discontinuous carbon fiber reinforced thermoplastics (DCFRTP) is considered as the favorable composite for applications on mass production vehicles because of the relatively high achievability for high cycle molding and complex shaped molding [1]. Consequently, randomly oriented strands (ROS), chopped carbon fiber tape reinforced thermoplastics (CTT) and other similar materials has recently attracted a lot of attention [2-9].

However, for complex shaped structures, such as L-shape, T-shape and hat-shape, which are frequently encountered in aerospace and automotive applications, the failure of such components is mainly due to delamination resulting from the out-of-plane stresses induced by the applied moment.

The interlaminar fracture energy release rate of fiber-reinforced composites can be measured for any of the three possible crack propagation modes: opening mode (Mode I), shear mode (Mode II) and tearing mode (Mode III), and Mode I is the most critical crack propagation mode because it has the lowest associated fracture energy release rate. Interlaminar failure of woven composites and unidirectional composites has been investigated by using numerical and experimental analysis [10-17]. However, despite the emergence of ROS as structural materials of mass-produced automobiles, studies on delamination behavior in ROS have yet to be reported. Therefore, Mode I delamination behavior for ultra-thin CTT (UT-CTT), which is ROS made of ultra-thin carbon fiber thermoplastic prepreg using a paper-making technique, were conducted in the present study.

In the present study, Mode I interlaminar behavior of UT-CTT was studied through experimental and numerical methods. Three different analytical calculation methods were used to evaluate the mode I energy release rate. Besides, the effects of interface stiffness, strength, and toughness were also investigated under the trapezoidal Cohesive Zone Model (CZM) law.

2. EXPERIMENT WORK

2.1 Materials characterization and testing setup

The UT-CTT samples were prepared from randomly oriented CF/PA6 ultra-thin unidirectional prepreg tapes. The tape was manufactured from carbon fibers (TR50S, Mitsubishi Rayon Co. Ltd., Japan) and polyamide 6 (PA6, Mitsubishi Plastics Co. Ltd., Japan); the tape measured 19 mm in length, 5 mm in width, 44 μm in thickness. The pre-crack was induced by inserting a 50 μm-thick polyimide film between the two middle layers before compression molding. The loading blocks were mounted on the top and bottom surfaces of the end of DCB specimen arms shown in Figure 1. Table 1 lists the dimensions of DCB specimens.

The DCB tests were performed according to guidelines in JIS K 8086 from the Japanese Industrial Standards Association [18]. Prior to testing, the edges of the DCB specimens were painted with typewriter correction fluid to assist visual crack length determination with a travelling microscope shown in Figure 2. The stroke speed was 1 mm min–1 for DCB tests using universal test machine (AUTOGRAPH AGS-5kN, Shimadzu Cooperation, Japan). During the DCB tests, two specimens were repeatedly loaded (in load, unload, and reload sequences) to accurately evaluate the compliance versus crack length.

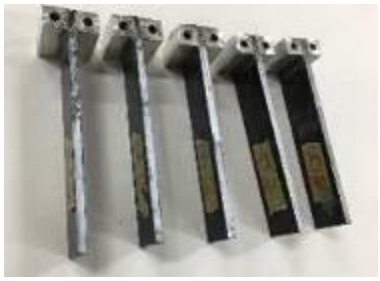

Figure 1: DCB specimens made of UT-CTT.

Figure 2: DCB test setup.

Specimen	DCB	
	Length×Width×Thickness ($L \times B \times 2T$)	a (mm)
E1	120 × 24 × 4.2	33.5
E2	120 × 24 × 4.2	36
E3	120 × 24 × 4.2	35
E4	120 × 24 × 4.2	35.5
E5	120 × 24 × 4.2	35

Table 1: Dimensions of DCB specimens.

2.2 Data analysis methods

For analysis of the test results three different calculation methods were used to estimate toughness, modified beam theory (MBT) method, modified compliance calibration (MCC) method and beam theory in reference to JIS K 7086 standard.

2.2.1 Modified beam theory (MBT) method

The Mode I interlaminar fracture toughness is calculated as follows:

$$G_{Ic,initiation}=\frac{3P\delta}{2B(a+\Delta)} \quad (1)$$

Where $G_{Ic,initiation}$ is the Mode I critical strain energy release rate for initiation of the crack, P is the load at the onset of crack growth, δ is the crack opening displacement at the point where the load P is applied and Δ can be found experimentally by plotting the cube root of compliance, $C^{1/3}$, as a function of crack length a.

2.2.2 Modified compliance calibration (MCC) method

In this method a least squares graph of the delamination length normalized by specimen thickness, $a/2T$, as a function of the cube root of compliance, $C^{1/3}$, is plotted using the visually observed delamination onset values and all the propagation values, the slope of this line is α_1 , C_0 is initial load point compliance of the specimen.

The Mode I interlaminar fracture toughness is calculated as follows:

$$G_{Ic,initiation}=\frac{3P^2C_0^{\frac{2}{3}}}{2\alpha_1 B(2T)} \quad (2)$$

2.2.3 Beam theory in reference to JIS K 7086 standard

According to JIS K 7086 standard, the critical load at the onset of crack growth P_c can be the load corresponding to 5% offset in initial compliance or at the load at visual observation of delamination onset at the edge. The Mode I interlaminar fracture toughness is evaluated using the Eq. (3) and (4) based on beam theory in reference to JIS K 7086 standard:

$$\frac{a}{2T} = \alpha_1 (BC)^{\frac{1}{3}} + \alpha_0 \tag{3}$$

$$G_{Ic,initiation} = \frac{3}{2(2T)} \left(\frac{P_c}{B}\right)^2 \frac{(BC_0)^{\frac{2}{3}}}{\alpha_1} \tag{4}$$

2.3 Results and discussion

The force-displacement curves of the DCB tests are presented in Figure 3. Unstable crack growth resulted in a saw-tooth like force–displacement curves after the initial stage of increasing load in the DCB tests. The initial bending stiffness of specimen E1 was higher than that of other specimens because the initial delamination length of E1 was slightly lower than those of others. However, the initial bending stiffness of specimen E2 was higher than that of the other specimens, which was unexpected because the initial delamination length of E2 was slightly larger than those of others; this can be explained by significant variations in the opening stiffness when the crack position was varied in the vicinity of the center of the DCB specimen [10]. In addition, the crack surfaces of the first UT-CTT DCB specimen and one of the unidirectional DCB specimens (for comparison purposes) were scanned by a 3D measurement macroscope. The thickness of UT-CTT and unidirectional DCB specimens are 4.2mm and 3mm, respectively. In Figure 4 and 5, the different colors represent the variation in height, and it can be seen clearly that the crack front of the UT-CTT DCB specimen was nearly straight, which is similar to the shape of the crack front of the unidirectional DCB specimen.

The initiation Mode I critical strain energy release rate determined by MBT, MCC and JIS K 7086 standard has been compared in Figure 6. The values determined by MBT and MCC differed by not more than 3 % which can be also seen in [19] while the value 3 N/mm calculated by JIS K 7086 standard is much lower because in this method the critical load at the onset of crack growth P_c can be the load corresponding to 5% offset in initial compliance while P is the maximum load in other two methods.

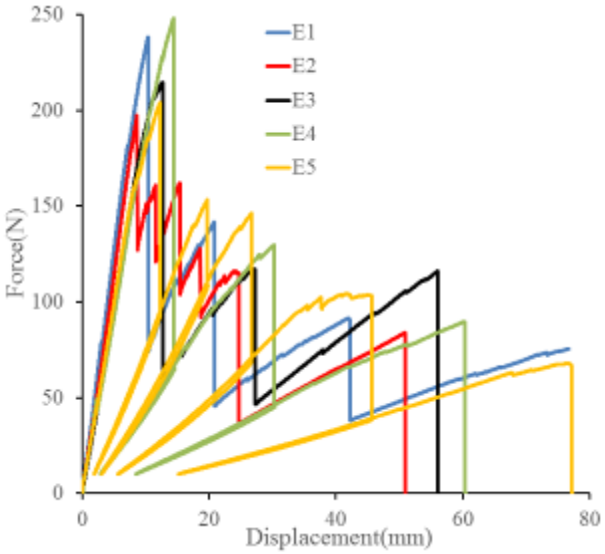

Figure 3: Force-displacement curves for DCB tests.

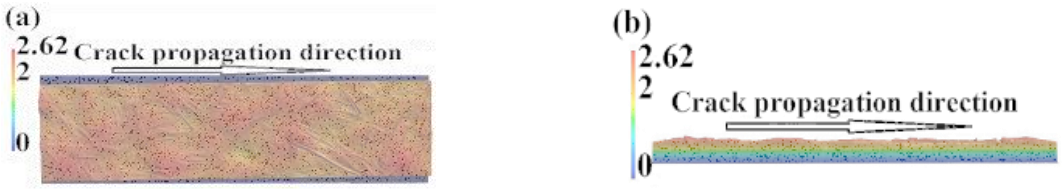

Figure 4: 3D measurement macroscope of crack propagation region in UT-CTT DCB specimen. (a)Top view (b)Side view.

Figure 5: 3D measurement macroscope of crack propagation region in unidirectional DCB specimen (a)Top view (b)Side view.

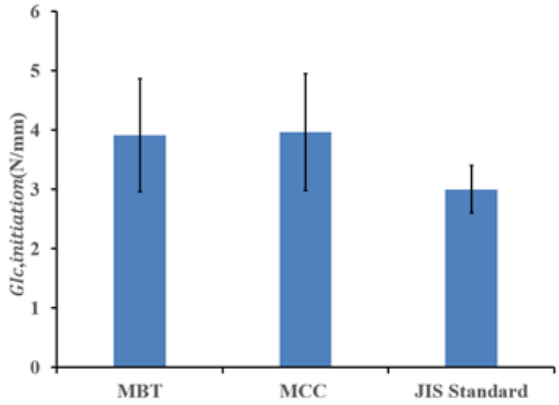

Figure 6: Initiation Mode I critical strain energy release rate with various data analysis methods.

3. NUMERICAL STUDY

3.1 Finite element models

Two-dimensional finite element models were developed in ABAQUS to simulate the delamination onset and propagation. The FE models were composed of four-node 2D plane strain elements. Surface-based cohesive contacts were inserted between two parts because the surface-based cohesive contact approach is an easier way than the cohesive element approach to model cohesive connections [20]. For the DCB tests, each composite plate was loaded at a speed of 1 mm min–1 at the appropriate nodes on loading blocks. A very refined mesh with the element size of 0.15 mm was used in a damage propagation zone in front of the crack tip; the mesh size was determined in the simulation of the DCB specimens after an investigation into the mesh dependence. Table 2 lists the mechanical properties of DCB specimens.

E1(GPa)	E2(GPa)	E3(GPa)	v12	G12(GPa)	G13(GPa)	G23(GPa)
41	41	3	0.28	16	1	1

Table 2: Mechanical properties of DCB specimens.

3.2 CZM implementation in the FE analysis

The CZM reproduced the elastic loading up to a peak load, damage onset, and crack growth due to local failure. In the present work, trapezoidal traction–separation shapes were evaluated. As shown in Figure 7, the trapezoidal CZM law is linear up to σ_0, where it goes through a range with constant stress, followed by a softening region before failure.

The interface stiffness K_i for Mode I of traction-separation law, which correlates traction to separation before crack onset, is defined as [21]:

$$K_I = \frac{\alpha E_3}{t} \tag{5}$$

A value of >50 for α is sufficiently accurate for most problems. In this study, α = 50.

The softening region in the trapezoidal CZM is defined by the damage variable and the effective displacement (δ_s) beyond damage initiation (δ_0). The value of the damage variable can be divided into the constant stress region ($\delta_0 < \delta \le \delta_s$) and the softening region ($\delta_s < \delta \le \delta_f$), as described in detail in [22].

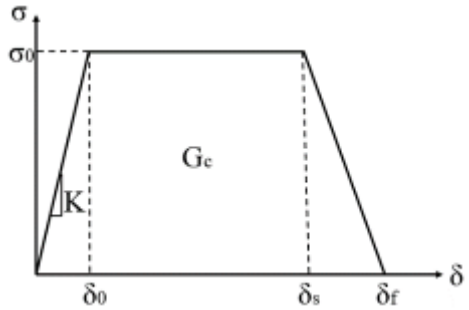

Figure 7: Trapezoidal traction-separation laws.

3.3 Numerical analysis results and discussion

The force–displacement curves with different interfacial parameters were compared with the experimental results; all force values were normalized to a width of 24 mm. Parametric studies were performed by independently varying interfacial strength and toughness by ±50%. Furthermore, in order to investigate the relationship between the shape of plastic zone and the specimen thickness, two DCB specimens with thickness 2.1 and 3mm were modeled. As shown in Figure 8, the shapes of plastic zone were almost the same during crack propagation.

Figure 9 shows the global force-displacement curves for DCB model with different interfacial stiffness, toughness and strength. The disagreement between the FE analysis results and experimental results after the first failure resulted from the mesh refinement in the damage propagation zone in front of the crack tip. However, the first failure corresponding to the peak force was the most important because the effects of interfacial parameters were considered in the study. The figures show that the effects of the interfacial stiffness on the peak force in force-displacement curves were negligible, while the interfacial stiffness became more sensitive during the crack propagation. Parametric studies on the interfacial toughness and strength showed that the peak force was sensitive to both the toughness and the strength. More specifically, the peak force changed by 25% when the interfacial toughness was changed by 50%, and it changed by 10% when the interfacial strength was changed by 50%.

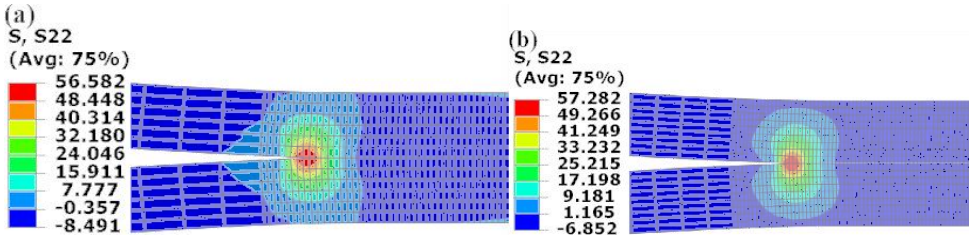

Figure 8: Distribution of through-thickness normal stress for DCB specimens. (a) t=2.1mm (b) t=3mm.

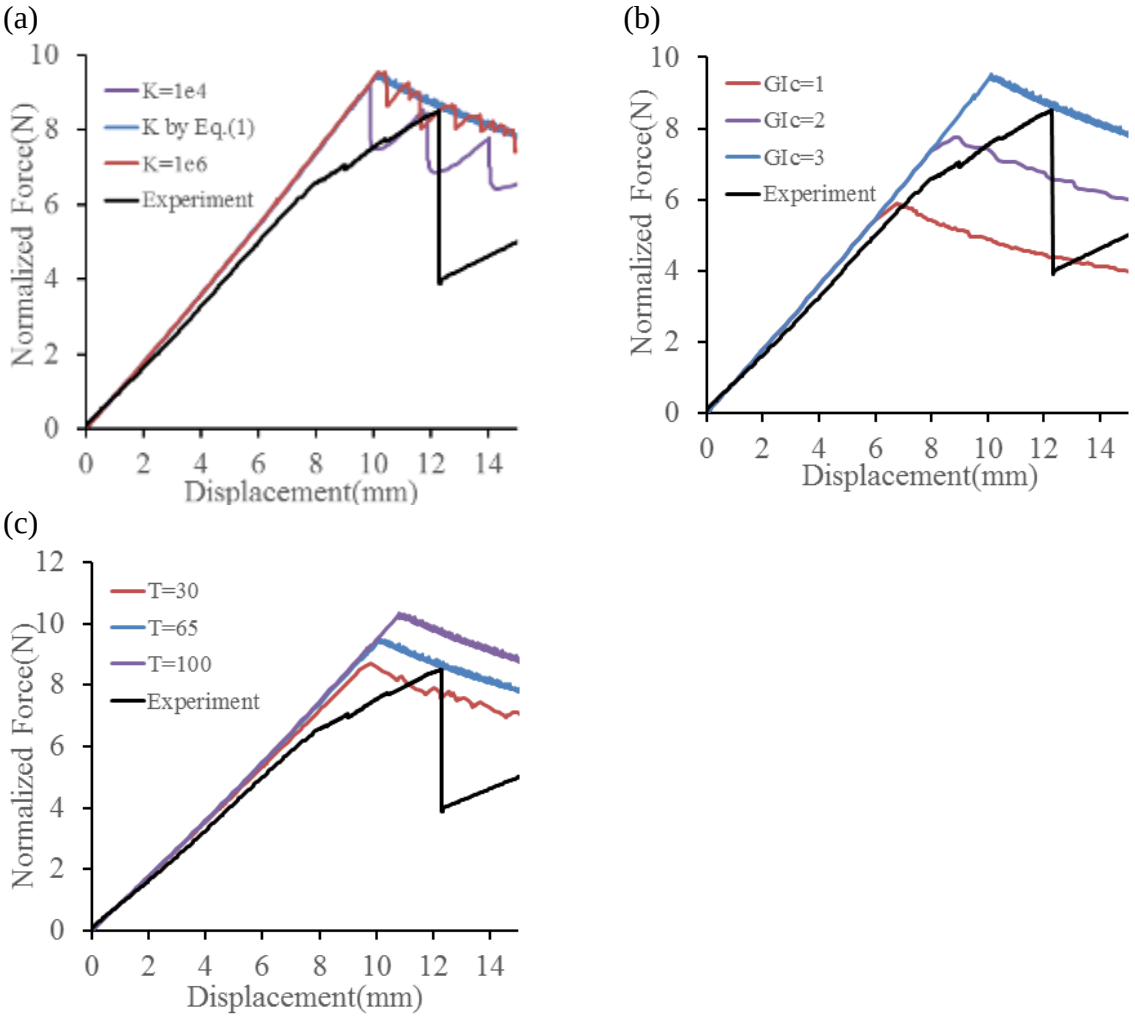

Figure 9: Force-displacement curves for the DCB case: (a) Effects of interfacial stiffness (b)Effects of interfacial toughness (c) Effect of interfacial strength.

4. CONCLUSION

This manuscript studied the interlaminar fracture toughness behavior of ultra-thin chopped carbon fiber tape reinforced thermoplastics (UT-CTT) under Mode I loading condition. To induce the mode I crack propagation, the Double Cantilever Beam (DCB) setup was considered. Unstable crack growth was observed resulting in a saw-tooth like force-displacement curve after initial increasing stage for DCB tests. Three different analytical calculation methods evaluating the mode I energy release rate

were compared and the value calculated by JIS K 7086 standard is much lower than other two methods.

In order to overcome convergence difficulties, a computationally efficient model using surface-based cohesive contact was developed to simulate delamination behavior. Parametric studies on the effects of the interfacial stiffness, strength and toughness on the global displacement force curves of UT-CTT showed that the model that used the trapezoidal traction-separation law was fairly insensitive to interfacial stiffness, but it was sensitive to both changes in the interfacial strength and toughness. In addition, the simulation results showed that the effect of the interfacial toughness on the peak force was much more sensitive than the effect of the interfacial strength.

ACKNOWLEDGEMENTS

Part of this study was conducted as Japanese METI project "the Future Pioneering Projects/ Innovative Structural Materials Project" since 2013fy. Authors would like to express sincerely appreciation to the project members who have provided valuable information and useful discussions.

REFERENCES

[1] Wan Y, Ohori T, Takahashi J. Mechanical properties and modeling of discontinuous carbon fiber reinforced thermoplastics, *Proceedings of the 20th International Conference on Composite Materials, Copenhagen, Denmark, July 19–24, 2015.*

[2] LeBlanc D, et al. Compression moulding of complex parts using randomly-oriented strands thermoplastic composites, *Proceedings of the SAMPE Technical Conference, Seattle, WA, USA, June 2–5, 2014*, Diamond Bar (CA): SAMPE, 2014. pp. 1–13.

[3] Selezneva, M. and L. Lessard, Characterization of mechanical properties of randomly oriented strand thermoplastic composites, *J. Compos. Mater*, **50**, 2016, pp. 2833-2851.

[4] Feraboli P, et al. Characterization of prepreg-based discontinuous carbon fiber/epoxy systems, *J. Reinf. Plast. Compos*, **28**, 2009, pp. 1191–1214.

[5] Lee H, et al. Applicability of FEM to complex shape parts made by ultra-thin chopped carbon fiber tape reinforced thermoplastics, *Proceedings of the 14th Japan International SAMPE Symposium and Exhibition, Kanazawa, Japan, December 6–9, 2015*.

[6] DeWayne D, Fukumoto S. Compression molding of long chopped fiber thermoplastic composites, *Proceedings of the CAMX 2014 Conference, Orlando, USA, October 13–16, 2014.*

[7] Feraboli P, et al. Modulus measurement for prepreg-based discontinuous carbon fiber/epoxy systems, *J. Compos. Mater*, **43**, 2009, pp. 1947–1965.

[8] Selezneva M, et al. Analytical model for prediction of strength and fracture paths characteristic to randomly oriented strand (ROS) composites, *Compos. Part B: Eng*, **96**, 2016, pp. 103–111.

[9] Eguemann N, et al. Compression moulding of complex parts for the aerospace with discontinuous novel and recycled thermoplastic composite materials, *Proceedings of the 19th International Conference on Composite Materials, Montréal, Québec, Canada, July 28–August 2, 2013*, pp. 6616–6626.

[10] De Baere I, et al. Study of the Mode I and Mode II interlaminar behaviour of a carbon fabric reinforced thermoplastic, *Polym. Test*, **31**, 2012, pp. 322–332.

[11] Miyagawa H, Sato C, Ikegami K. Effect of fiber orientation on mode I fracture toughness of CFRP, *J. Appl. Polym. Sci*. **115**, 2010, pp. 3295–3302.

[12] Ivanov S, Gorbatikh L, Lomov S. Interlaminar fracture behaviour of textile composites with thermoplastic matrices, *Proceedings of the 16th European Conference on Composite Materials, Seville, Spain, June 22–26, 2014*.

[13] Schon J, et al. A numerical and experimental investigation of delamination behaviour in the DCB specimen, *Compos. Sci. Technol*, **60**, 2000, pp. 173–184.

[14] Wang W-X, et al. Experimental investigation on test methods for mode II interlaminar fracture testing of carbon fiber reinforced composites, *Compos. Part A: Appl. Sci. Manuf*, **40**, 2009, pp. 1447–1455.

[15] Schön J, et al. Numerical and experimental investigation of a composite ENF-specimen, *Eng. Fract. Mech*, **65**, 2000, pp. 405–433.
[16] Zabala H, et al. Loading rate dependency on mode I interlaminar fracture toughness of unidirectional and woven carbon fiber epoxy composites, *Compos. Struct*. **121**, 2015, pp. 75–82.
[17] Ma Y, et al. A study on the failure behavior and mechanical properties of unidirectional fiber reinforced thermosetting and thermoplastic composites, *Compos. Part B: Eng*, **99**, 2016, pp. 162–172.
[18] Japanese Standards Association. *Testing methods for interlaminar fracture toughness of carbon fibre reinforced plastics*, Tokyo: Japanese Standards Association, JIS K 7086, 1993.
[19] Prasad, M.S., C. Venkatesha, and T. Jayaraju, Experimental methods of determining fracture toughness of fiber reinforced polymer composites under various loading conditions, *J. Min. Mater. Chara. Eng*, **10**, 2011, pp. 1263-1275.
[20] Simulia, D., *ABAQUS 6.11 analysis user's manual*, 2011.
[21] Turon A, et al. An engineering solution for mesh size effects in the simulation of delamination using cohesive zone models, *Eng. Fract. Mech*, **74**, 2007, pp. 1665–1682.
[22] Campilho R, et al. Modelling adhesive joints with cohesive zone models: effect of the cohesive law shape of the adhesive layer, *Int. J. Adhes. Adhes*, **44**, 2013, pp. 48–56.